Journal of Applied Polymer Science

Crystallization of Isotactic Polypropylene inside Dense Networks of Carbon Nanofillers

Jing-Bin Chen,[1] Jia-Zhuang Xu,[1] Huan Pang,[1] Gan-Ji Zhong,[1] Ling Xu,[1] Hu Tang,[1] Jian-Hua Tang,[2] Zhong-Ming Li[1]

[1]College of Polymer Science and Engineering and State Key Laboratory of Polymer Materials Engineering, Sichuan University, Chengdu 610065, China

[2]College of Chemical Engineering, Sichuan University, Chengdu 610065, China

Correspondence to: G.-J. Zhong (E-mail: ganji.zhong@scu.edu.cn) or Z.-M. Li (E-mail: zmli@scu.edu.cn)

ABSTRACT: In this study, we performed the crystallization of carbon nanotube (CNT)/isotactic polypropylene (iPP) and graphene nanosheet (GNS)/iPP composites with very high nanofiller loadings; these are frequently used in polymer composites for electromagnetic interference shielding and thermal conductivity. Rheology testing indicated that both the high-loading CNTs and GNSs formed dense networks in the iPP matrix, and transmission electron microscopy showed that their connection types were completely different: the CNTs contacted one another in a dot-to-dot manner, whereas the GNSs linked reciprocally in a plane-to-plane manner. The carbon nanofiller networks brought about two opposite effects on iPP crystallization: a nucleation effect and a confinement effect. The CNT network showed a stronger nucleation effect; however, the CNT network also revealed a more powerful confinement effect because the CNT network was denser than the GNS network. With increasing content of the carbon nanofillers, the crystallization rates of both the CNT and GNS composites first increased, then decreased, and showed a very high saturation concentration at 50 wt %; this resulted from the competitive relationship between the nucleation effect and confinement effect. The crystallization was facilitated when the carbon nanofiller concentration was below saturation, where the nucleation effect invariably played a dominant role. Although the crystallization was depressed when the carbon nanofiller concentration was above saturation, the nucleation effect was subdued, and the confinement effect was extensive. Compared to the GNS/iPP composites, the CNT/iPP composites showed a more depressed crystallization. The suppression mechanism is discussed with consideration of the local topological structure constructed by those two carbon nanofillers. © 2013 Wiley Periodicals, Inc. J. Appl. Polym. Sci. **2014**, *131*, 39505.

KEYWORDS: composites; crystallization; graphene and carbon nanofillers; polyolefins

Received 20 March 2013; accepted 3 May 2013

DOI: 10.1002/app.39505

INTRODUCTION

Polymeric composites based on carbon nanotubes (CNTs) and graphene nanosheets (GNSs), because of their outstanding physical and mechanical properties, have attracted increasing attention.[1–5] It has been found that many physical behaviors of the polymer matrix, such as the glass transition,[6] phase separation,[7] and crystallization,[8,9] are dramatically altered through the incorporation of carbon nanofillers, which eventually have a significant influence on the properties of the ultimate composites, that is, the mechanical properties,[10–12] thermal conductivity,[13] and electromagnetic shielding properties.[14,15] In addition, the structural characteristics of CNTs and GNSs and their physical interactions originating from their high aspect ratios and high specific surface areas are closely related to the phase behaviors and properties of carbon nanofiller/polymer composites.[16,17]

The crystallization behavior of CNT-based and GNS-based polymer composites, as one of most important aspects in the field of polymeric phase behavior, has been widely investigated. CNTs, because of their quasi-one-dimensional structure, large aspect ratio, and enormous surface energy, have been extensively accepted as one of the most effective nucleating agents for various semicrystalline polymers.[8,18,19] For example, the onset crystallization temperature (T_0) of isotactic polypropylene (iPP), which contains a relatively low CNT loading of 0.1 wt %, was increased by about 9°C.[20] Even at a CNT loading as low as 0.02 wt %, the crystallization half-time ($t_{1/2}$) of poly(L-lactide) can decrease acutely to 9.6%.[21] Polycarbonate, usually viewed as an amorphous polymer, was unexpectedly found to form a crystalline structure in the existence of CNTs.[22] In addition to improving the crystallization kinetics of polymers, CNTs can also induce a special crystalline morphology, that is, a nanohybrid shish-kebab structure, which may effectively improve the

interfacial stress transfer and directly optimize the mechanical properties of polymer composites.[23–25] For GNSs, it has been reported that they can also accelerate polymer crystallization as effective nucleating agents.[26–28] For instance, in our previous work, the $t_{1/2}$ of iPP containing 0.05 wt % GNSs was reduced by at least 50% compared with that of neat iPP, and the acceleration phenomenon was more obvious when the GNSs presented a synergistic effect with shear.[29] Furthermore, the crystallization rate of polyethylene composites containing 0.4 vol % GNSs was one to two orders of magnitude greater than neat polyethylene.[30] Although both CNTs and GNSs can induce polymer crystallization, a significant morphological difference exists between CNTs and GNSs, where GNSs, made up of one or several atom layers, are viewed as two-dimensional (2D) nanoplates, and CNTs, consisting of curled graphite layers with two half-fullerenes capping either end of the tube, can be regarded as one-dimensional (1D) nanolines; these structures lead to differences in the nucleation abilities of these two carbon nanofillers. A comparative study on the CNT- and GNS-induced isothermal crystallization of poly(L-lactide) at relatively low contents (0.05 and 0.1 wt %) showed that the crystallization rate of CNT/poly(L-lactide) composites was much faster than that of GNS/poly(L-lactide) composites; this results in a simpler induction process and a larger space for the growth of crystals in CNT-based composites compared with the GNS-based ones.[31] A molecular dynamics simulation study also confirmed this dimensionality effect of carbon nanofillers on the crystallization of alkane.[32]

In most previous works, the concentration of carbon nanofillers has been selected to be as low as possible to highlight the outstanding nucleation effect of carbon nanofillers. However, to achieve desirable properties, such as electromagnetic interference shielding, thermal conductivity, and mechanical properties, it is necessary to add high loadings of carbon nanofillers to polymer matrices.[33,34] For instance, to meet the electric requirements in practical applications, high loadings of conductive carbon nanofillers are usually demanded to form abundant conductive paths in polymer matrices; this transforms insulators to conductors.[1,35] The formation of a network at a high carbon nanofiller content can improve the thermal conductivity of polymers remarkably, which is usually very hard to tune.[36] Moreover, polymer composites combining high-content carbon nanofillers have revealed amazing enhancements in the thermoelectric performance and mechanical properties compared with neat polymers.[37,38] With regard to the aspect of crystallization behavior, high-loading carbon nanofillers not only offer a larger density of heterogeneous nucleation sites but also bring marked confinement to the polymer chain mobility during crystallization,[39] which is much more complex than that of low-loading carbon nanofiller systems. Thereby, the results obtained from polymer composites at low carbon nanofiller contents may not represent the results obtained for the same polymer composites at a high carbon nanofiller contents. Additionally, high-loading carbon nanofillers usually construct dense networks in the polymer matrix, and different dimensional carbon nanofillers may form networks with diverse structural features; this may result in a discrepancy in the polymer crystallization. In a recent study, we found that the crystallization of ethylene–vinyl acetate copolymers was constrained in the presence of CNT and GNS networks with different structural features, and the GNS network more seriously suppressed the crystallization of ethylene–vinyl acetate than the CNT one.[40,41]

In this study, after our previous findings of the enhanced nucleation ability of iPP by very low loadings of carbon nanofillers, the crystallization behaviors of CNT/iPP and GNS/iPP composites with a series of high carbon nanofiller loadings were investigated to obtain more insight into the crystallization of iPP in the presence of carbon nanofillers. Our results show that the content and dimensionality of carbon nanofillers have obvious influences on the nucleation ability and crystallization rate of iPP; this was different from the situation in the low-loading system.

EXPERIMENTAL

Materials

The iPP (trademarked as T30s) used in this study was provided by Dushanzi Petroleum Chemical Co., China, with a melt flow index of 3 g/10 min (230°C, 2.16 kg), weight-average molecular weight of 39.9×10^4 g/mol, and weight-average molecular weight/number-average molecular weight of 4.6. The CNTs were provided by Chengdu Organic Chemicals Co., Ltd., and the Chinese Academy of Sciences R&D Center for Carbon Nanotubes. The CNTs had a length of 10–20 μm and an outer diameter of 30–50 nm. The GNSs were synthesized from expanded graphites by the modified Hummers method, and detailed information, such as electrical and mechanical properties, of the as-prepared GNSs can be found in previous articles.[42,43] Expandable graphite, with an expansion rate of 200 mL/g at 800°C, was purchased from Qingdao Haida Graphite Co., Ltd. (China). Xylene (analytical-reagent grade) and *N,N*-dimethylformamide (DMF; analytical-reagent grade) were provided by Chengdu Kelong Chemical Reagent Factory (China) and were used as received.

Preparation of the CNT/iPP and GNS/iPP Composites

A solution dispersion process was used to prepare the iPP composites. High carbon nanofiller contents were selected: 5, 20, 50, and 70 wt %. Taking the 5 wt % CNT/iPP composite as an example, the experimental procedure was as follows: 0.25 g of CNTs was added to 100 mL of DMF, and the suspension was subjected to ultrasound and mechanical stirring for 90 min to obtain a uniform dispersion. At the same time, iPP (4.75 g) was completely dissolved in xylene (400 mL) at 140°C. When we dropped the stable CNT/DMF suspension into the iPP/xylene solution, the coagulated material precipitated continuously. Thereafter, ethanol was poured into the mixture until no more coagulated material precipitated. The coagulates made up of the CNT/iPP composites were transferred to evaporating dishes, left at room temperature for 24 h, and then dried in a vacuum at 80°C for 48 h to evaporate any residual solvent. For the preparation of the GNS/iPP composite, the reduction of graphene oxide nanosheets was carried out in hydrazine at 95°C for 3 h.[44] The CNT/iPP composites with 5, 20, 50, and 70 wt % CNTs are noted as PPCN5, PPCN20, PPCN50, and PPCN70, respectively, and the GNS/iPP composites with 5, 20, 50 and 70 wt % GNS are noted as PPGN5, PPGN20, PPGN50, and PPGN70, respectively. The neat iPP is indicated as PP0.

Transmission Electron Microscopy (TEM) Observation

The morphology of the as-prepared CNT/iPP and GNS/iPP composites were characterized by TEM with an acceleration voltage of 200 kV (FEI Tecnai F20). Thin sections of the iPP composites with a thickness of about 80 nm for TEM observations were prepared with a Leica EMUC6/FC6 microtome at −100°C.

Differential Scanning Calorimetry (DSC) Measurements

DSC measurements were performed on a TA DSC Q200 instrument. About 5 mg of dried sample was heated to 180°C at a heating rate of 20°C/min and held at this temperature for 5 min to eliminate the thermal history. Then, the sample was cooled to 80°C at a constant cooling rate (2, 5, or 10°C/min) for the study of nonisothermal crystallization. The crystallization kinetics study was based on isothermal crystallization, which was monitored according to the following procedures: the samples were first annealed at 180°C for 5 min to erase thermal history and then cooled to 140°C at a cooling rate of 40°C/min. All of the experiments were carried out in a nitrogen atmosphere. To reveal the growth geometry of crystals during isothermal crystallization, the Avrami equation was adopted:

$$\ln[-\ln(1-X(t))] = n\ln t + \ln k \quad (1)$$

where $X(t)$ is the relative crystallinity of the materials at a certain isothermal crystallization time (t) and n and k are the Avrami exponent and the kinetic rate constant, respectively. The crystallization half-time ($t_{1/2}$), which represents the crystallization rate, was obtained with the following equation:

$$t_{1/2} = [\ln 2/k]^{1/n} \quad (2)$$

Dynamical Rheology Testing

The viscoelastic properties of the CNT/iPP and GNS/iPP composites were studied with a stress controlled dynamic rheometer AR2000ex (TA Instruments) with a parallel-plate geometry. The CNT/iPP and GNS/iPP composites were compression-molded into disks with a thickness of 1 mm and a diameter of 25 mm at 190°C and 10 MPa. The dynamic rheological tests of these samples were then conducted at 210°C under a nitrogen atmosphere. Frequency sweeps between 0.1 and 100 rad/s were carried out at a low strain (2%), which was within the linear elastic range for these materials.

X-Ray Diffraction (XRD) Characterization

XRD patterns of the samples were taken on a Rigaku diffractometer (Japan) with Cu Kα radiation at a wavelength of 0.1542 nm. The measurements were taken at a scanning rate of 3.6°/min. Before the test, the samples were isothermally crystallized at 140°C with a Linkam CSS-450 high-temperature shearing stage to be consistent with the DSC measurements. The overall crystallinity (X_c) was calculated by the following equation:

$$X_c = \frac{\sum A_{\text{cryst}}}{\sum A_{\text{cryst}} + \sum A_{\text{amorp}}} \quad (3)$$

where A_{cryst} and A_{amorp} represent the fitted areas of the crystalline and amorphous phases, respectively.

RESULTS

Nonisothermal Crystallization of the CNT/iPP and GNS/iPP Composites

The nonisothermal crystallization exothermic DSC curves of the CNT/iPP and GNS/iPP composites at various cooling rates are shown in Figure 1. The DSC endotherms exhibited only one crystallization peak, which was dependent on the CNT and GNS loadings and the cooling rate. From these curves, T_0 and the crystallization peak temperature (T_p) were obtained, and these are shown in Table I. For each sample, the higher cooling rate made T_0 and T_p shift to lower temperatures; this is common in the nonisothermal crystallization of semicrystalline polymers.[45] The presence of CNTs and GNSs moved T_0 and T_p of iPP toward higher temperatures, regardless of the cooling rate. This indicated the strong heterogeneous nucleation effects of the CNTs and GNSs on the crystallization of iPP. The iPP chains may have been attached to the surfaces of the carbon nanofillers through the intermolecular CH–π interaction between iPP and the carbon nanofillers; as a result, the surface energy of iPP nucleation could have been reduced, and thus iPP crystallized at higher temperatures during nonisothermal crystallization.[46,47]

The nonisothermal crystallization behavior of the two types of iPP composites showed similar tendencies. The values of T_0 and T_p first increased and then decreased with increasing CNT and GNS loadings, with maximum values at 50 wt %. This indicated 50 wt % CNTs or GNSs, at a very high loading, caused the strongest nucleation ability for iPP. At a selected content, T_0 and T_p were higher in the CNT/iPP composites than in the GNS/iPP composites. For example, compared with PP0, T_0 and T_p for PPCN50 increased by 16.8 and 17.1°C, respectively, at a cooling rate of 5°C/min, whereas these values increased by only 9.6 and 9.4°C, respectively, for PPGN50. This definitely indicated that the CNTs acted as more effective heterogeneous nucleating agents than the GNSs. The stronger heterogeneous nucleation effect of the CNTs may have been due to the 1D topological structure, which brought a simpler induction approach to iPP crystallization.[31]

Isothermal Crystallization of the CNT/iPP and GNS/iPP Composites

The crystallization kinetics of the CNT/iPP and GNS/iPP composites were investigated by isothermal crystallization. Figure 2 shows $X(t)$ as a function of the crystallization time for the CNT/iPP and GNS/iPP composites isothermally crystallized at 140°C. All these curves had a similar sigmoid shape. Apparently, the time to complete the crystallization of iPP was extensively reduced by the incorporation of the carbon nanofillers. This confirmed that high loadings of carbon nanofillers, because of their outstanding nucleation abilities, markedly accelerate the overall crystallization rate of iPP. At the same crystallization time and the same carbon nanofiller content, the $X(t)$ value of the CNT/iPP composites was much higher than that of the GNS/iPP composites; this indicated that the 1D CNTs were more efficient at accelerating the crystallization of iPP than the 2D GNSs. In addition, it is worth mentioning that for both the CNT/iPP and CNT/iPP composites, the crystallization rates sped up immediately, then decelerated with carbon nanofiller

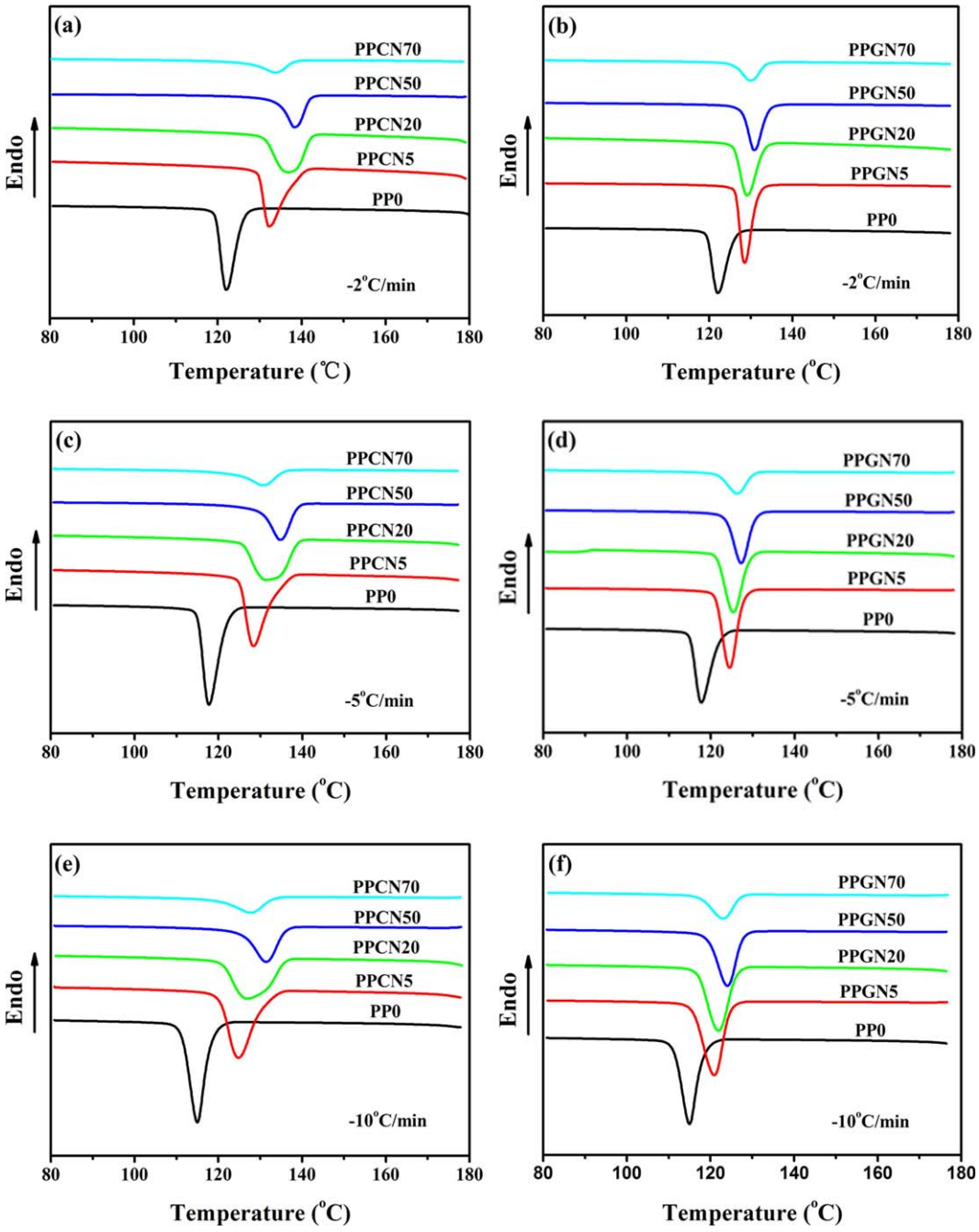

Figure 1. Nonisothermal crystallization thermograms of the (a,c,e) CNT/iPP and (b,d,f) GNS/iPP composites at cooling rates of 2, 5, and 10°C/min. [Color figure can be viewed in the online issue, which is available at wileyonlinelibrary.com.]

content, and showed maxima at PPCN50 and PPGN50; this implied that the crystallization of iPP was confined when the carbon nanofiller loading was higher than 50 wt %.

The isothermal crystallization kinetics of the CNT/iPP and GNS/iPP composites were analyzed further by the Avrami equation [eq. (1)]. Figure 3 shows the plots of $\ln\{-\ln[1-X(t)]\}$ versus $\ln(t)$ for the CNT/iPP and GNS/iPP composites isothermally crystallized at 140°C, in which n stands for the growth dimension of crystals that could be obtained, as listed in Table II. The value of n was 3.64 for PP0, whereas it declined into the ranges 1.88–2.20 for the CNT/iPP composites and 2.68–3.38 for the GNS/iPP composites, respectively. This indicated that the growth of the iPP crystals was confined by the CNTs and GNSs. The change in n showed a carbon nanofiller content dependence, in which n of the CNT/iPP composites always decreased ahead of the GNS/iPP composites and had a greater reduction than that of the GNS/iPP composites. For example, compared with PP0, PPCN5 displayed a drastically decreased n (2.03) as did PPCN70 ($n = 1.91$), although PPGN5 showed a slightly depressed n (3.38), and the diminution was

Table I. T_0 and T_p Values of the CNT/iPP and GNS/iPP Composites at Various Cooling Rates

	T_0 (°C)			T_p (°C)		
Sample	2°C/min	5°C/min	10°C/min	2°C/min	5°C/min	10°C/min
PP0	124.9	121.0	117.7	122.0	117.8	115.0
PPCN5	138.6	134.2	131.1	132.2	128.4	124.8
PPCN20	140.9	137.2	133.9	136.8	131.4	126.9
PPCN50	141.1	137.8	134.9	138.4	134.9	131.6
PPCN70	138.2	135.6	133.1	133.7	130.5	127.6
PPGN5	131.6	127.7	124.6	128.4	124.5	120.9
PPGN20	133.2	129.2	126.2	129.0	125.4	121.9
PPGN50	134.2	130.6	127.7	130.8	127.2	124.0
PPGN70	133.7	130.1	127.2	129.9	126.2	123.0

more obvious in PPGN70 ($n = 2.68$). Because of the numerous CNTs and GNSs used in this study, carbon nanofiller networks were likely to form in the iPP matrix; this could have caused a confinement effect on the iPP crystal growth. It was clear that the growth dimension of the iPP crystals immediately decreased when CNTs were added to iPP; however, the growth dimension

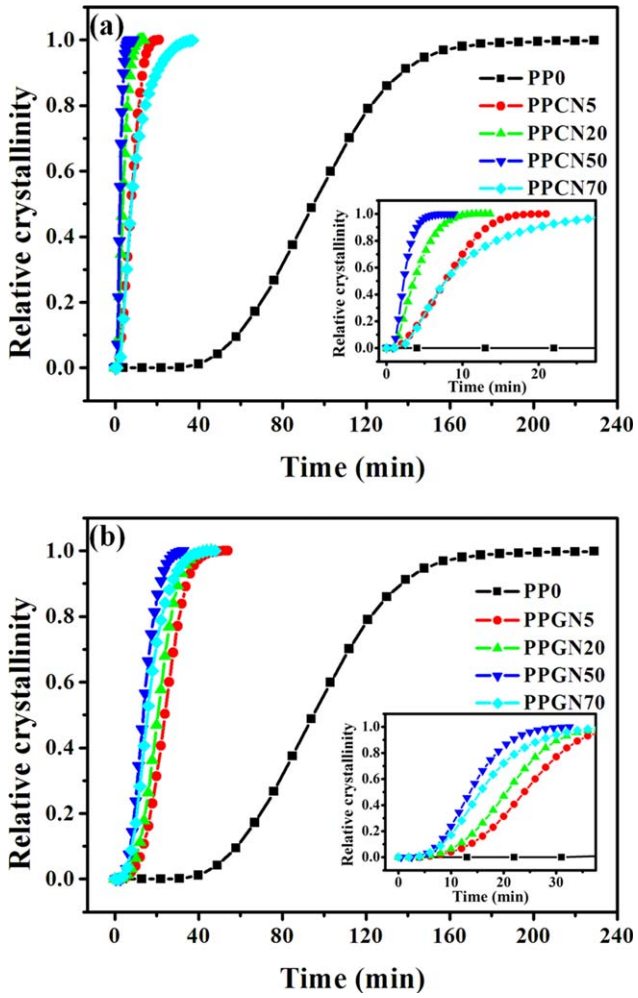

Figure 2. Plots of $X(t)$ versus the crystallization time for the (a) CNT/iPP and (b) GNS/iPP composites crystallized isothermally at 140°C. The insets show the amplifications of the curves. [Color figure can be viewed in the online issue, which is available at wileyonlinelibrary.com.]

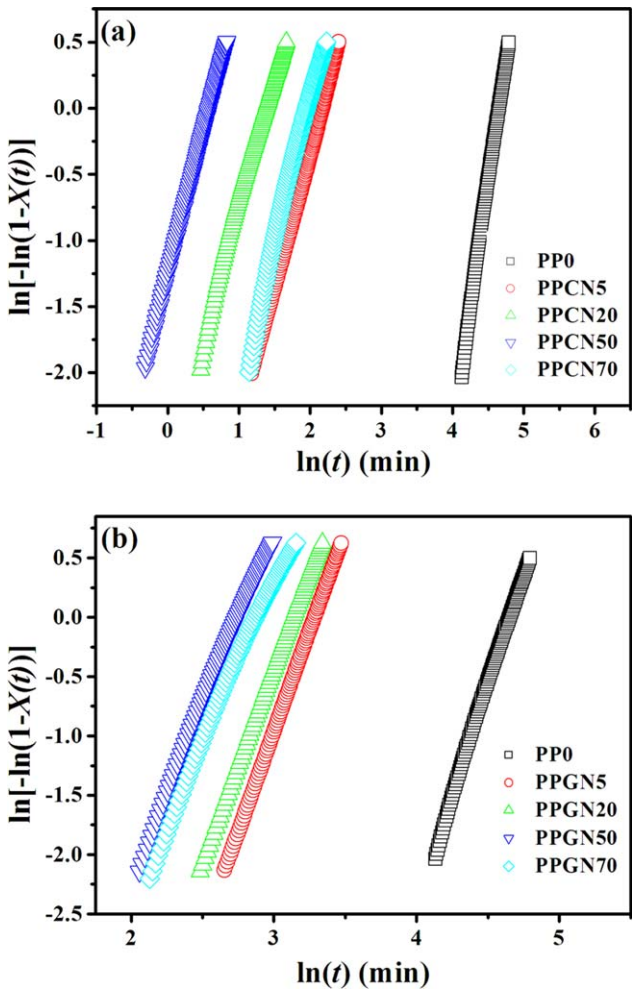

Figure 3. Avrami plots for the (a) CNT/iPP and (b) GNS/iPP composites with carbon nanofiller contents during isothermal crystallization at 140°C. [Color figure can be viewed in the online issue, which is available at wileyonlinelibrary.com.]

Table II. Values of *n* for the CNT/iPP and GNS/iPP Composites with Different Carbon Nanofiller Contents during Isothermal Crystallization at 140°C

Sample	n	Sample	n
PP0	3.64	PP0	3.64
PPCN5	2.03	PPGN5	3.38
PPCN20	1.88	PPGN20	3.24
PPCN50	2.20	PPGN50	2.88
PPCN70	1.91	PPGN70	2.68

of iPP crystals gradually decreased with the GNS content. This may have been related to the different abilities for CNTs and GNSs to construct a dense network.

According to eq. (2), $t_{1/2}$, which is a measure of crystallization rate, could be calculated. Figure 4 shows the $t_{1/2}$ values of the CNT/iPP and GNS/iPP composites isothermally crystallized at 140°C. Compared to PP0, $t_{1/2}$ for the CNT/iPP and GNS/iPP composites was greatly reduced; this suggested an obviously accelerated overall crystallization rate of iPP in the existence of CNTs or GNSs. For instance, $t_{1/2}$ decreased from 96.93 min for PP0 to 2.06 min for PPCN50 and 13.15 min for PPGN50; these values represented 98 and 86% reductions, respectively. Additionally, $t_{1/2}$ of the CNT/iPP composites was always lower than that of the GNS/iPP composites at the same carbon nanofiller loading; this verified that the CNTs were more conducive to accelerating the crystallization of iPP. We also observed, as shown in Figure 4, that for both the CNT/iPP and GNS/iPP composites with CNT and GNS contents below 50 wt %, $t_{1/2}$ showed a downward trend, whereas at a loading of 70 wt %, $t_{1/2}$ increased compared to that of PPCN50 and PPGN50. Therefore, we concluded that the saturation CNT and GNS contents to promote the iPP crystallization kinetics was 50 wt %; this was much higher than the saturations reported in other

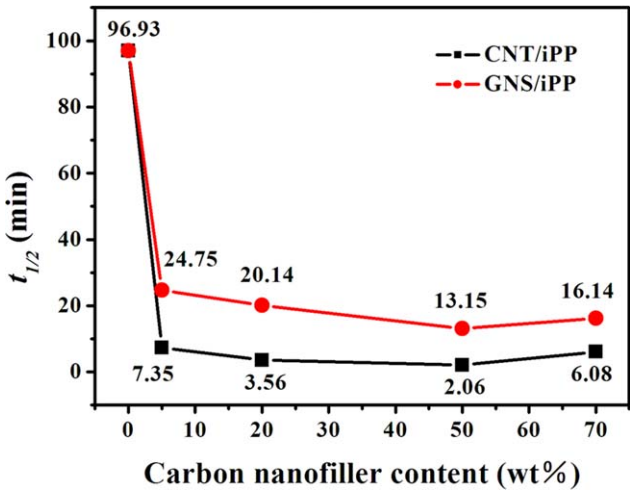

Figure 4. Changes in $t_{1/2}$ of the CNT/iPP and GNS/iPP composites with carbon nanofiller contents at an isothermal crystallization temperature of 140°C. [Color figure can be viewed in the online issue, which is available at wileyonlinelibrary.com.]

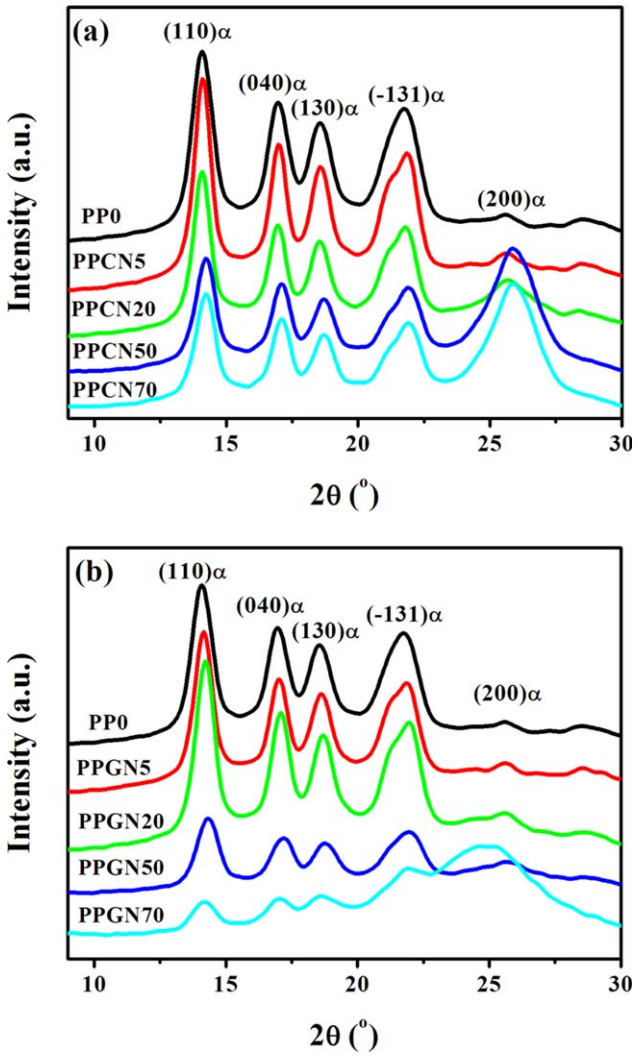

Figure 5. XRD curves of the (a) CNT/iPP and (b) GNS/iPP composites with different carbon nanofiller contents after the isothermal crystallization at 140°C. [Color figure can be viewed in the online issue, which is available at wileyonlinelibrary.com.]

studies.[48–52] For instance, a similar saturation was also observed at a relatively low content (7.4 wt %) in the CNT/iPP composite; this could be attributed to the alkyl-modified CNTs, which led to a better carbon nanofiller dispersion in iPP than that in our study.[39] The carbon nanofiller content dependence of the crystallization kinetics suggested that the dense degree of network formed at a high loading of carbon nanofillers may be an important factor in influencing the crystallization of iPP. Moreover, $t_{1/2}$ of PPCN70 was 6.08 min; this was almost 2.5 times that of PPCN50, whereas $t_{1/2}$ of PPGN70 only showed a limited increase compared to PPGN50. This indicated that PPCN70 showed a more serious depression of iPP crystallization than PPGN70; this may have been related to the different structures of the CNT and GNS networks.

Crystalline Structure of the CNT/iPP and GNS/iPP Composites

Figure 5 shows the XRD patterns of CNT/iPP and GNS/iPP composites isothermally crystallized at 140°C. All of the systems

Table III. Crystallinity Values of the CNT/iPP and GNS/iPP Composites with Different Carbon Nanofiller Contents after Isothermal Crystallization at 140°C

Sample	X_c (%)	Sample	X_c (%)
PP0	54.1	PP0	54.1
PPCN5	52.3	PPGN5	54.6
PPCN20	53.1	PPGN20	51.7
PPCN50	57.2	PPGN50	52.3
PPCN70	56.8	PPGN70	54.2

presented the same characteristic diffracting peaks corresponding to the planes (110), (040), (130), (−131), and (200) of the α form. There were not any other crystalline forms; this indicated that the CNTs and GNSs were the α-crystal nucleating agent of iPP. It can also be seen in Figure 5 that the intensity of plane (200) increased with carbon nanofiller content, especially at ultrahigh loadings; this suggests that a high loading of carbon nanofillers encouraged the α-crystal growth of iPP along the normal of plane (200). The X_c values of the CNT/iPP and GNS/iPP composites were calculated according to eq. (3) and are summarized in Table III. As shown in Table III, X_c of iPP did not change obviously in the presence of carbon nanofillers, even though the crystallization rate of iPP was distinctly influenced by the carbon nanofillers.

DISCUSSION

The previous results definitely demonstrated that high loadings of CNTs and GNSs could act as effective nucleating agents to accelerate the iPP crystallization, and the nucleation ability of the CNTs was stronger than that of the GNSs. This was similar to the situation of the case of low loading; however, both the nucleation ability and overall crystallization rate of iPP first increased and then decreased with the CNT and GNS content and showed saturations at a carbon nanofiller loading of 50 wt %. The largest difference between the superlow (~0.1 wt %) and superhigh (>5.0 wt % in this study) carbon nanofiller loadings was the formation of crowded carbon nanofiller networks. To examine the formation of the CNT and GNS networks, the rheological behavior of the iPP composites was measured, as shown in Figure 6.

The rheological result strongly proves the formation of the CNT and GNS networks. As shown in Figure 6, both the CNT/iPP and GNS/iPP composites displayed elevated storage modulus values in comparison to PP0, especially in the low-frequency region; this suggested that the interactions between the carbon nanofillers and iPP chains slowed down the motion of the iPP chains.[51] With increasing frequency, PP0 had a drastic sensitivity of the storage modulus to the frequency, whereas the CNTs and GNSs depressed the frequency dependence. Particularly, the storage modulus values of PPCN20 and PPGN20 already reached plateaus at low frequencies; this suggested that the CNTs and GNSs formed networks in the composites containing 20 wt % carbon nanofillers. We also found, as shown in Figure 6, that the values of the storage modulus of the CNT/iPP composites were always higher than those of the GNS/iPP composites at the same carbon nanofiller loading; this implied that the iPP chains suffered more powerful restrictions in the CNT networks than in the GNS networks. Because it was hard to determine accurate storage modulus values of the composites with CNT and GNS contents higher than 20 wt %, TEM observation of the composites containing 50 wt % carbon nanofillers was carried out to explore the internal structures of the CNT and GNS networks.

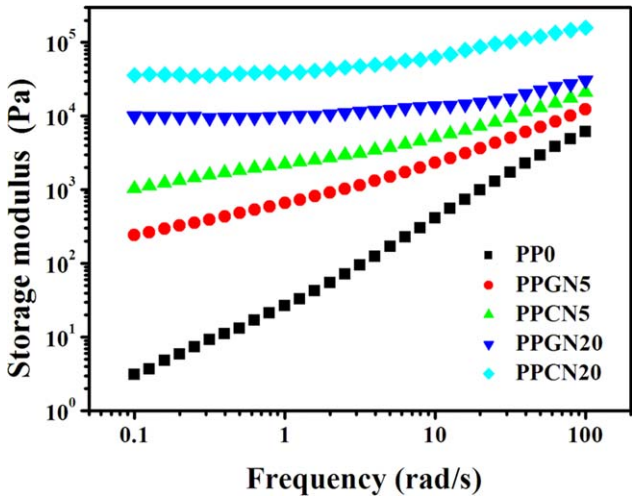

Figure 6. Storage modulus as a function of the frequency for the CNT/iPP and GNS/iPP composites with different carbon nanofiller contents. Rheological measurements were performed with a strain of 2% at 210°C. [Color figure can be viewed in the online issue, which is available at wileyonlinelibrary.com.]

Figure 7 shows typical TEM images with a carbon nanofiller content of 50 wt %. One can clearly see that both the CNTs and GNSs were very crowded and in contact with each other to form a dense network in the iPP matrix. However, because of the different dimensional characteristics of the CNTs and GNSs, the structural features of their networks were quite different. The connection type between the 1D nanoline-like CNTs was apparently dot to dot [see the inset in Figure 7(a)], whereas mainly plane-to-plane connections between the 2D nanoplate-like GNSs are shown in Figure 7(b). Because is easier to reduce the surface area of GNSs than that of CNTs because of the plane-to-plane connections,[53] the interfacial area in the GNS/iPP composites was lower than that of the CNT/iPP composites at the same content of carbon nanofillers; this may have led to the higher storage modulus in the CNT/iPP composites, as shown in Figure 6. The different type of network connection may have also led to various dense degrees of the networks. Compared to the 1D CNTs, the GNSs may have much more difficult to interlace with each other to form a dense network with the plane-to-plane connection.[53] A denser network may have also resulted in a higher storage modulus in the CNT/iPP composites. Thus, combining the structural difference of the carbon nanofillers and the rheological results, we concluded that the CNT networks were denser than the GNS networks.

From the traditional crystallization point of view, crystallization consists of two stages: nucleation and crystal growth. Nucleation is the precondition for crystallization, and crystal growth is

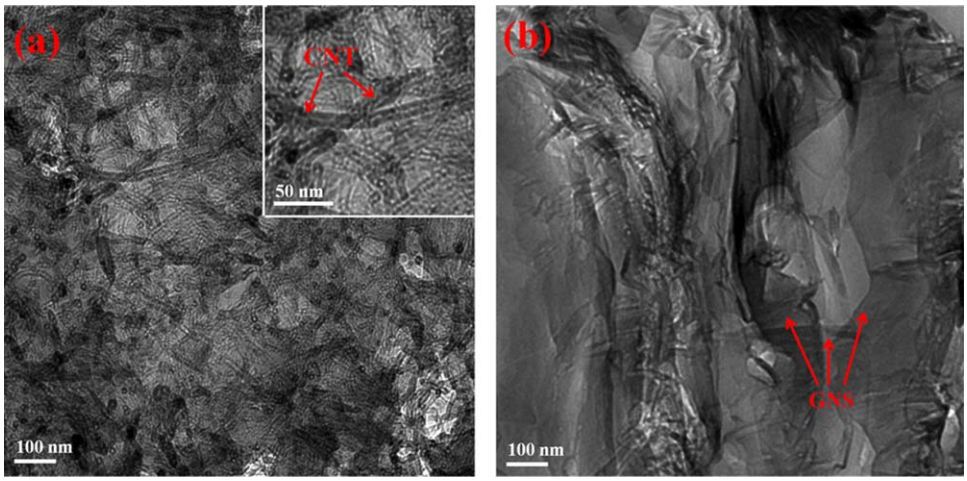

Figure 7. TEM images of (a) PPCN50 and (b) PPGN50 prepared by a solution dispersion processing. [Color figure can be viewed in the online issue, which is available at wileyonlinelibrary.com.]

related to mobility of the chains, the formation kinetics of a certain modification, and the growth space. Both the CNTs and GNSs acted as effective heterogeneous nucleating agents. When the CNTs and GNSs were added to iPP, the nucleation density of iPP was promoted; this led to a conspicuous decrease in the distances between the adjacent nucleation sites. Thereby, the growth of the iPP crystals was finished quickly when adjacent crystals were in contact with each other, and this shortened the crystallization period and resulted in a smaller $t_{1/2}$.

It is necessary to discuss the origin of the CNT- and GNS-network-induced crystallization of iPP to get more insight into the various abilities of these two carbon nanofiller networks with differently structural features to change iPP crystallization. According to previous studies, the topological structures of the carbon nanofillers had a significant effect on the carbon-nanofiller-induced polymer crystallization,[46,54,55] whereas our results also show local different topological structures of carbon nanofiller networks, which had an obvious influence on the crystallization of iPP. From these results, the high loading of CNTs were more efficient than that of the GNSs in accelerating polymer crystallization. This phenomenon was in line with the case of superlow CNT and GNS loadings.[31,32] A possible reason is that compared to the GNSs, the CNTs had simpler nucleation procedures and larger carbon nanofiller surfaces for the iPP crystallization.

It was reported that a nanofiller network formed in the polymer matrix may bring a confinement effect to extensively hinder the mobility and diffusion of polymer chains to crystal growth fronts; this slows down polymer crystallization.[56,57] In this study, at a relatively low carbon nanofiller content (e.g., 5 wt %), both the CNTs and GNSs revealed remarkable heterogeneous nucleation abilities; this led to obvious improvements in T_0, T_p, and the overall crystallization rate. When the carbon nanofiller content was increased to 50 wt %, the nucleation sites provided by the carbon nanofillers were improved routinely; thus, the T_0 and T_p values of the composites continuously increased (see Table I). Simultaneously, the carbon nanofiller networks forced a rigorous confinement on the motion and diffusion of the iPP chains; this was confirmed by the rheological measurements. Hence, the carbon nanofiller networks brought two opposite effects, that is, a nucleation effect and a confinement effect, on the crystallization of iPP, and the overall crystallization rate was determined by the mutual counteractivity of those two effects. For the composites containing carbon nanofiller contents below 50 wt %, the nucleation effect invariably played a dominant role; this led to the continuous acceleration of the crystallization rate (see Figure 4). Although when the carbon nanofiller content increased from 50 to 70 wt %, the carbon nanofiller networks become denser, and the surface connections between the carbon nanofillers become more frequent; this may have led to the situation in which the available nucleation sites of the carbon nanofillers for PPCN70 (or PPGN70) were less numerous than those for PPCN50 (or PPGN50). Consequently, the nucleation abilities of PPCN70 and PPGN70 were weaker than those of PPCN50 and PPGN50, respectively (see Table I). Meanwhile, denser carbon nanofiller networks brought more serious confinement effects to the iPP crystallization. Thus, compared to PPCN50 (or PPGN50), the crystallization rate of PPCN70 (or PPGN70) decreased as a result of the cooperation of the decreased nucleation effect and extensive confinement effect.

In a comparison of $t_{1/2}$ values of the composites containing 50 and 70 wt % carbon nanofillers, PPCN70 showed a more obvious crystallization rate decrease compared to PPGN70. These different results were attributed to the following reasons. On the one hand, the CNT/iPP composites showed a more obvious T_p drop (see Table I) when the carbon nanofiller content was increased from 50 to 70 wt %; this indicated that the recession of the nucleation effect of the CNTs was more excessive. On the other hand, compared to the GNS network, the CNT network became more dense and forced stronger confinement effect on the iPP crystallization with increasing carbon nanofiller content more easily. The 1D CNTs, because of their tubular structure, were much easier to insert into the loose network to obtain a denser network, whereas the 2D GNSs were difficult to form a denser network as a result of the restriction of the large lateral areas.[53]

It is certain that the value of *n*, being representative of the crystal growth dimension, is related to the crystallization kinetics of iPP. A decrease in the *n* values demonstrates that the crystal growth of polymers is restricted.[58] It has been reported earlier that the combination of carbon nanofillers can reduce the crystal growth dimension of polymers.[3,49] Complicated reasons may lead to the restriction of iPP crystal growth, but the most likely three are presented as follows:

1. CNTs and GNSs serve as 1D and 2D templates (nuclei) for iPP crystal growth so that the initial consumption of the iPP melt is 1D or 2D in nature.
2. Because of the compact nucleation sites on the CNTs or GNSs surfaces, the growth of the iPP crystals is confined between the adjacent crystals.
3. Because of the networks formed in the matrix, the evolution of iPP crystals is confined in the limited spaces. Because the CNT network is denser than the GNS network, CNTs bring more intense spatial confinement to the iPP crystal growth than GNSs.

In the CNT/iPP composites, the CNT network was dense enough to restrain the growth of iPP crystals; this limited the growth dimensionality of the iPP crystals. Hence, *n* for the CNT/iPP composites was dramatically decreased compared with that of PP0. However, unlike with the 1D CNTs, the large lateral areas of the 2D GNSs determined that the GNS network was looser than the CNT network at the same carbon nanofiller content. Therefore, in the composites containing a relatively low GNS content (e.g., 20 wt %), the GNS network was not dense enough to bring rigid spatial confinement to the iPP crystallization; this resulted in only a slightly decreased *n* compared with PP0. Only when the GNS content further increased (e.g., 50 and 70 wt %) did the GNS network become dense enough to force a more rigorous spatial confinement to iPP crystallization; this led to obvious decreases in *n*.

CONCLUSIONS

The effects of networks formed by differently topological carbon nanofillers on the crystallization behavior of iPP were comparatively investigated; two kinds of carbon nanofillers (CNTs and GNSs) were selected as candidates for incorporation into iPP to form networks. The connection type was dot to dot in the CNT network, whereas it was mainly plane to plane in the GNS network. Both the CNTs and GNSs in the networks could act as effective heterogeneous nucleating agents to accelerate the crystallization of iPP, whereas the CNTs showed stronger nucleation abilities than the GNSs. For both the CNT/iPP and GNS/iPP composites, the nucleation ability and crystallization rate of iPP increased with the carbon nanofiller content and then decreased when the content exceeded the saturation value (50 wt %); this resulted from the competitive relation between the nucleation effect and the confinement effect of the carbon nanofiller networks. When the carbon nanofiller content was below saturation, the nucleation effect invariably played a predominant role; this led to the continuous acceleration of the crystallization rate with the carbon nanofiller content. Although when the carbon nanofiller content was higher than saturation, the nucleation effect was subdued, and the confinement effect was extensive; this resulted in the depression of crystallization. Compared to the GNS network, the CNT network revealed a more excessive recession of the nucleation effect and a more conspicuous increase in the confinement effect; this caused a more serious depression of crystallization in the CNT/iPP composites.

ACKNOWLEDGMENTS

This study was supported by the National Outstanding Youth Foundation of China (contract grant number 50925311), the National Natural Science of China (contract grant number U1162131), the Foundation for Innovative Research Groups of the National Natural Science Foundation of China (contract grant number 51121001), the Open Foundation of Top Priority Subjects of Zhejiang Province (contract grant number 20110903), and the Specialized Research Fund for the Doctoral Program of Higher Education (contract grant number 20120181120101).

REFERENCES

1. Stankovich, S.; Dikin, D. A.; Dommett, G. H. B.; Kohlhaas, K. M.; Zimney, E. J.; Stach, E. A.; Piner, R. D.; Nguyen, S. B. T.; Ruoff, R. S. *Nature* **2006**, *442*, 282.
2. Coleman, J. N.; Khan, U.; Blau, W. J.; Gun'ko, Y. K. *Carbon* **2006**, *44*, 1624.
3. Moniruzzaman, M.; Winey, K. I. *Macromolecules* **2006**, *39*, 5194.
4. Teng, C. C.; Ma, C. C. M.; Yang, S. Y.; Chiou, K. C.; Lee, T. M. *J. Appl. Polym. Sci.* **2012**, *123*, 888.
5. Wang, D. W.; Li, F.; Zhao, J.; Ren, W.; Chen, Z. G.; Tan, J.; Wu, Z. S.; Gentle, I.; Lu, G. Q.; Cheng, H. M. *Am. Chem. Soc. Nano* **2009**, *3*, 1745.
6. Ding, N.; Chen, X. F.; Wu, C. M. L.; Lu, X. Q. *J. Phys. Chem. C* **2012**, *116*, 22532.
7. Wongsuwarn, S.; Ji, Y.; Cicuta, P.; Terentjev, E. M. *Soft Matter* **2013**, *9*, 235.
8. Grady, B. P.; Pompeo, F.; Shambaugh, R. L.; Resasco, D. E. *J. Phys. Chem. B* **2002**, *106*, 5852.
9. Augustine, J. M.; Maiti, S. N.; Gupta, A. K. *J. Appl. Polym. Sci.* **2012**, *125*, 478.
10. Koval'chuk, A. A.; Shchegolikhin, A. N.; Shevchenko, V. G.; Nedorezova, P. M.; Klyamkina, A. N.; Aladyshev, A. M. *Macromolecules* **2008**, *41*, 3149.
11. Chaudhry, A. U.; Mittal, V. *Polym. Eng. Sci.*, to appear.
12. Dubnikova, I.; Kuvardina, E.; Krasheninnikov, V.; Lomakin, S.; Tchmutin, I.; Kuznetsov, S. *J. Appl. Polym. Sci.* **2010**, *117*, 259.
13. Tseng, I. H.; Lin, H. C.; Tsai, M. H.; Chen, D. H. *J. Appl. Polym. Sci.* **2012**, *126*, 182.
14. Arjmand, M.; Apperley, T.; Okoniewski, M.; Sundararaj, U. *Carbon* **2012**, *50*, 5126.
15. Zhang, H. B.; Yan, Q.; Zheng, W. G.; He, Z.; Yu, Z. Z. *Am. Chem. Soc. Appl. Mater. Interfaces* **2011**, *3*, 918.
16. Gao, H.; Song, L.; Guo, W. H.; Huang, L.; Yang, D. Z.; Wang, F. C.; Zuo, Y. L.; Fan, X. L.; Liu, Z.; Gao, W.; Vajtai, R.; Hackenberg, K.; Ajayan, P. M. *Carbon* **2012**, *50*, 4476.

17. Wurstbauer, U.; Schiros, T.; Jaye, C.; Plaut, A. S.; He, R.; Rigosi, A.; Gutiérrez, C.; Fischer, D.; Pfeiffer, L. N.; Pasupathy, A. N.; Pinczuk, A.; Garcia, J. M. *Carbon* **2012**, *50*, 4822.
18. Bhattacharyya, A. R.; Sreekumar, T.; Liu, T.; Kumar, S.; Ericson, L. M.; Hauge, R. H.; Smalley, R. E. *Polymer* **2003**, *44*, 2373.
19. Zhu, S. Y.; Zhao, Y. Y.; Qiu, Z. B. *J. Appl. Polym. Sci.* **2012**, *124*, 4268.
20. Lu, K.; Grossiord, N.; Koning, C. E.; Miltner, H. E.; Mele, B.; Loos, J. *Macromolecules* **2008**, *41*, 8081.
21. Xu, H. S.; Dai, X. J.; Lamb, P. R.; Li, Z. M. *J. Polym. Sci. Part B: Polym. Phys.* **2009**, *47*, 2341.
22. Sung, Y. T.; Kum, C. K.; Lee, H. S.; Byon, N. S.; Yoon, H. G.; Kim, W. N. *Polymer* **2005**, *46*, 5656.
23. Li, L. Y.; Li, C. Y.; Ni, C. Y. *J. Am. Chem. Soc.* **2006**, *128*, 1692.
24. Kawakami, D.; Burger, C.; Ran, S. F.; Avila-Orta, C.; Sics, I.; Chu, B.; Chiao, S. M.; Hsiao, B. S.; Kikutani, T. *Macromolecules* **2008**, *41*, 2859.
25. Keum, J. K.; Burger, C.; Zuo, F.; Hsiao, B. S. *Polymer* **2007**, *48*, 4511.
26. Xu, J. Z.; Liang, Y. Y.; Huang, H. D.; Zhong, G. J.; Lei, J.; Chen, C.; Li, Z. M. *J. Polym. Res.* **2012**, *19*, 9975.
27. Xu, J. Z.; Liang, Y. Y.; Zhong, G. J.; Li, H. L.; Chen, C.; Li, L. B.; Li, Z. M. *J. Phys. Chem. Lett.* **2012**, *3*, 530.
28. Jing, X. J.; Qiu, Z. B. *Ind. Eng. Chem. Res.* **2012**, *51*, 13686.
29. Xu, J. Z.; Chen, C.; Wang, Y.; Tang, H.; Li, Z. M.; Hsiao, B. S. *Macromolecules* **2011**, *44*, 2808.
30. Cheng, S.; Chen, X.; Hsuan, Y. G.; Li, C. Y. *Macromolecules* **2011**, *45*, 993.
31. Xu, J. Z.; Chen, T.; Yang, C. L.; Li, Z. M.; Mao, Y. M.; Zeng, B. Q.; Hsiao, B. S. *Macromolecules* **2010**, *43*, 5000.
32. Yang, J. S.; Yang, C. L.; Wang, M. S.; Chen, B. D.; Ma, X. G. *Phys. Chem. Chem. Phys.* **2011**, *13*, 15476.
33. Layek, R. K.; Samanta, S.; Chatterjee, D. P.; Nandi, A. K. *Polymer* **2010**, *51*, 5846.
34. Thostenson, E. T.; Ren, Z.; Chou, T. W. *Compos. Sci. Technol.* **2001**, *61*, 1899.
35. Pang, H.; Yan, D. X.; Bao, Y.; Chen, J. B.; Chen, C.; Li, Z. M. *J. Mater. Chem.* **2012**, *22*, 23568.
36. Haggenmueller, R.; Guthy, C.; Lukes, J. R.; Fischer, J. E.; Winey, K. I. *Macromolecules* **2007**, *40*, 2417.
37. Chen, J. K.; Gui, X. C.; Wang, Z. W.; Li, Z.; Xiang, R.; Wang, K. L.; Wu, D. H.; Xia, X. G.; Zhou, Y. F.; Wang, Q. *Am. Chem. Soc. Appl. Mater. Interfaces* **2011**, *4*, 81.
38. Liu, Y. T.; Dang, M.; Xie, X. M.; Wang, Z. F.; Ye, X. Y. *J. Mater. Chem.* **2011**, *21*, 18723.
39. Xu, D. H.; Wang, Z. G. *Polymer* **2008**, *49*, 330.
40. Pang, H.; Zhong, G. J.; Xu, J. Z.; Yan, D. X.; Ji, X.; Li, Z. M.; Chen, C. *Chin. J. Polym. Sci.* **2012**, *30*, 879.
41. Pang, H.; Zhong, G. J.; Wang, Y.; Xu, J. Z.; Li, Z. M.; Lei, J.; Chen, C.; Ji, X. *J. Polym. Res.* **2012**, *19*, 9837.
42. Dikin, D. A.; Stankovich, S.; Zimney, E. J.; Piner, R. D.; Dommett, G. H. B.; Evmenenko, G.; Nguyen, S. B. T.; Ruoff, R. S. *Nature* **2007**, *448*, 457.
43. Pang, H.; Chen, T.; Zhang, G.; Zeng, B.; Li, Z. M. *Mater. Lett.* **2010**, *64*, 2226.
44. Ren, P. G.; Yan, D. X.; Ji, X.; Chen, T.; Li, Z. M. *Nanotechnology* **2011**, *22*, 055705.
45. Ke, Y. C.; Wu, T. B.; Xia, Y. F. *Polymer* **2007**, *48*, 3324.
46. Hu, X.; An, H.; Li, Z. M.; Geng, Y.; Li, L.; Yang, C. *Macromolecules* **2009**, *42*, 3215.
47. Li, J.; Fang, Z. P.; Tong, L. F.; Gu, A. J.; Liu, F. *Eur. Polym. J.* **2006**, *42*, 3230.
48. Ferreira, C. I.; Dal Castel, C.; Oviedo, M. A. S.; Mauler, R. S. *Thermochim. Acta* **2012**, *553*, 40.
49. Li, L.; Li, C. Y.; Ni, C.; Rong, L.; Hsiao, B. *Polymer* **2007**, *48*, 3452.
50. Xu, D. H.; Wang, Z. G.; Douglas, J. F. *Macromolecules* **2008**, *41*, 815.
51. Xu, Z. H.; Niu, Y. H.; Wang, Z. G.; Li, H.; Yang, L.; Qiu, J.; Wang, H. *Am. Chem. Soc. Appl. Mater. Interfaces* **2011**, *3*, 3744.
52. Wang, H. S.; Qiu, Z. B. *Thermochim. Acta* **2012**, *527*, 40.
53. Du, J. H.; Zhao, L.; Zeng, Y.; Zhang, L. L.; Li, F.; Liu, P. F.; Liu, C. *Carbon* **2011**, *49*, 1094.
54. Tanaka, F. *Macromolecules* **2000**, *33*, 4249.
55. Varshney, V.; Carri, G. A. *Macromolecules* **2005**, *38*, 780.
56. Gam, S.; Meth, J. S.; Zane, S. G.; Chi, C.; Wood, B. A.; Seitz, M. E.; Winey, K. I.; Clarke, N.; Composto, R. *J. Macromolecules* **2011**, *44*, 3494.
57. Xu, Z. H.; Niu, Y. H.; Yang, L.; Xie, W. Y.; Li, H.; Gan, Z. H.; Wang, Z. G. *Polymer* **2010**, *51*, 730.
58. Xu, J. T.; Wang, Q.; Fan, Z. Q. *Eur. Polym. J.* **2005**, *41*, 3011.